A&A 409, 1017–1030 (2003)
DOI: 10.1051/0004-6361:20031161

Astronomy & Astrophysics

Magnetic activity of six young solar analogues
II. Surface Differential Rotation from long-term photometry

S. Messina[1,⋆] and E. F. Guinan[2]

[1] Catania Astrophysical Observatory, INAF, Via S. Sofia 78, 95123 Catania, Italy
[2] Dept. of Astronomy and Astrophysics, Villanova University, Villanova 19085, PA, USA
e-mail: edward.guinan@villanova.edu

Received 16 May 2003 / Accepted 18 July 2003

Abstract. The present paper is the second of a series dedicated to the study of the magnetic activity in a selected sample of young solar analogues. The sample includes five single G0-G5V stars with ages between ≃130 Myr and 700 Myr: EK Dra, π^1 UMa, HN Peg, k^1 Cet and BE Cet. In this study we also include the Pleiades-age (≃130 Myr) K0V star DX Leo. Our analysis is based on high precision photometric observations carried out as part of *The Sun in Time* project, aimed at a multiwavelength study of stars with solar-like global properties, but with different ages and thus at different stages of evolution. In the first paper of this series we presented the photometric observations and determined the existence of starspot cycles and their correlation with the global stellar properties. In the present paper we investigate the surface differential rotation (SDR). The periodogram analysis of the photometric data time series has allowed us to determine the rotational periods and to derive the following results: *i)* all the selected stars show variations of the rotational period. Such variations are definitely periodic and in phase with the starspot cycle for BE Cet and DX Leo. They are likely periodic and in phase also for π^1 UMa, EK Dra and HN Peg, but still need confirmation. By analogy with the solar butterfly diagram, the rotational period variations are interpretable in terms of surface differential rotation, that is, they are attributable to the existence of active latitude belts migrating during the activity cycle on a differentially rotating star; *ii)* BE Cet, π^1 UMa and EK Dra show a solar-like pattern of SDR, that is the rotational period steadily decreases along the activity cycle, jumping back to higher values at the beginning of the next cycle; on the contrary, DX Leo, k^1 Cet and HN Peg show an antisolar pattern; *iii)* the amplitude of the rotational period variations shows a power law dependence on the rotational period similar to that found in previous studies. Contrary to theoretical predictions, the cycle length is not correlated to the Dynamo number, it is indeed positively correlated to the SDR amplitude. More precisely, stars tend to concentrate along three different branches with the cycle length increasing with increasing $\Delta\Omega/\Omega$. Moreover, we found that the SDR amplitude changes from cycle to cycle, which is reminiscent of a wave of excess rotation propagating in latitude; *iiii)* the apparently different solar and antisolar behaviours are probably due to different inclinations of the stellar rotation axis under which the star is seen. The long-term photometry of the young single star LQ Hya, although not included in the initial project, is also used in the present analysis to enlarge the investigated sample. We determined for LQ Hya three different starspot cycles and an antisolar pattern of SDR.

Key words. stars: activity – stars: late-type – stars: magnetic fields – stars: rotation – stars: starspots

1. Introduction

Stars with solar-like global properties (e.g., mass, $T_{\rm eff}$, $L/L_\odot$), but at different stages of evolution, are suitable to study the evolution of the Sun's magnetic activity. With this aim coordinated multiwavelength observations of several nearby, single, solar-type stars selected as proxies for the Sun from the ZAMS (Zero Age Main Sequence) to the TAMS (Terminal Age Main Sequence) have been carried out since 1990 as part of *The Sun in Time* project. The aim of the project is to investigate stellar activity cycles and differential rotation, to determine the evolution of the solar dynamo and magnetic activity as well as to extract the solar UV and X-ray fluxes through the Sun's post-ZAMS history (Dorren & Guinan 1994; Güdel et al. 1997; Guinan et al. 2001). In the first paper of this series (Messina & Guinan 2002, hereafter referred to as Paper I) we presented the photometric observations and determined the existence of starspot cycles and of correlations between cycle length, amplitude and global stellar properties for a selected sample of six young solar analogues. In the present paper we investigate the presence of Surface Differential Rotation (SDR) and its connection with the starspot cycle in the same sample of stars, that is five young single G0-G5V stars with ages between ≃130 Myr

Send offprint requests to: S. Messina,
e-mail: sme@ct.astro.it

⋆ Guest User, Canadian Astronomy Data Center, which is operated by the Dominion Astrophysical Observatory for the National Research Council of Canada's Herzberg Institute of Astrophysics.

Table 1. Name and stellar properties (Cols. 1–5) of program stars and of eight additional stars, three of which with known starspot cycles and SDR and five with known cycles and SDR from CaII H&K measurements; shortest and longest observed rotation periods (Col. 6) taken from Tables 2 to 8; mean period (Col. 7) and amplitude of the surface differential rotation (Col. 8). The starspot cycle periods (P_{cyc}) of program stars are taken from Paper I (Cols. 9–11). In Col. 12 the sources for cycles and rotation periods of additional stars as well as the labels to identify the stars in Figs. 3–5 are given.

Name	Sp. T.	V (mag)	$B-V$ (mag)	τ_c (d)	P_{min}–P_{max} (d)	$\overline{P}_{rot}$ (d)	$\frac{\Delta P}{\overline{P}_{rot}}$	$P_{cyc1} \pm \Delta P$ (yr)	$P_{cyc2} \pm \Delta P$ (yr)	$P_{cyc3} \pm \Delta P$ (yr)	Label/Ref.
Program stars											
BE Cet	G2 V	6.36	0.66	12.33	7.405–8.030	7.756	0.081[a]	6.7 ± 0.7	–	–	A
k^1 Cet	G5 V	4.80	0.68	13.27	9.045–9.406	9.214	0.039[b]	5.9 ± 0.2	–	–	B
π^1 UMa	G1.5 V	5.63	0.62	10.43	4.543–5.385	4.905	0.171[a]	13.1 ± 0.9	2.12 ± 0.05	–	C
EK Dra	G0 V	7.51	0.61	9.96	2.551–2.886	2.682	0.125[a]	9.2 ± 0.4	>30	–	D
HN Peg	G0 V	5.94	0.59	9.03	4.59–5.17	4.84	0.120[b]	5.5 ± 0.3	–	–	E
DX Leo	K0 V	7.01	0.76	16.86	5.345–5.476	5.424	0.024[b]	3.21 ± 0.05	–	–	F
Additional single stars with known SDR from photometry											
AB Dor	K0 V	6.89	0.83	19.61	0.5133–0.5225	0.5179	0.017[a]	18.30	5.9	–	G/1
LQ Hya	K2 V	7.74	0.90	21.87	1.5938–1.6154	1.6042	0.013[b]	3.2	6.2	11.4	H
Sun	G2 V	–	0.66	11.9	24.5–28.5	26.09	0.153[a]	10.5	84	44	S/2
Additional single stars with known SDR from Ca II H&K											
107 Psc	K1V	5.14	0.84	20.0	34.0–37.3	35.2	0.094[b]	9.6	–	–	I/2
61 UMa	G8V	5.30	0.72	15.1	16.13–17.62	16.68	0.089[c]	—	>25	–	L/2
β Com	F9.5V	4.30	0.58	8.6	10.6–13.1	12	0.208[a]	16.6	9.6	–	M/3
HD 160346	K3V	6.50	0.96	23.4	35.4–37.8	36.4	0.066[a]	7.0	>25	–	N/2
15 Sge	G1V	5.79	0.61	10.0	12.67–15.57	13.94	0.208[b]	2.6	16.9	–	O/2

1: Collier Cameron & Donati (2002); 2: Donahue et al. (1996); 3: Gray & Baliunas (1997); [a] star with solar-like pattern of SDR; [b] star with antisolar pattern of SDR; [c] star with hybrid pattern of SDR.

and 700 Myr: EK Dra, π^1 UMa, HN Peg, k^1 Cet and BE Cet. We also include in this study the Pleiades-age (≃130 Myr) K0V star DX Leo (see Table 1).

A good knowledge of the SDR and of its dependence on the global stellar properties is remarkable as differential rotation is one of the key ingredients of the hydromagnetic dynamo in the generation and sustainment of stellar magnetic fields. These are thought to be responsible of all activity phenomena observed in late-type stars (see e.g. Guinan & Giménez 1992; Catalano et al. 1999; Rodonò 2000). Moreover, observational studies of stellar differential rotation are fundamental since they provide empirical relations which allow us to test dynamo theories. In fact, also the current solar dynamo models are not capable yet to successfully reproduce the temporal and spatial properties of the magnetic fields observed at the Sun's surface (Stix 1984).

Since it is not possible to resolve the stellar disk, the measurements of differential rotation currently derived from stellar observations are indirect. Nonetheless, they are indicative of the conditions in the stellar interior and put significant constraints to the amplitude of the internal differential rotation, the last being the quantity used in the models.

Measurements of stellar SDR are currently obtained in different ways: from Doppler Imaging maps, by latitude-by-latitude cross-correlation analysis to pairs of surface images obtained several days apart (Vogt & Penrod 1983); from χ^2 landscape imaging methods (Collier Cameron et al. 2002; Donati et al. 2000); from line profile analysis (Reiners & Schmitt 2002); from stellar butterfly diagrams, that is from the season-to-season variations of the rotational period, as measured from spectro-photometric (e.g. Ca II H&K fluxes, Wilson 1978; Baliunas et al. 1985, 1995; Dohanue et al. 1996) or broad-band photometric observations, and correlated with the phase of the stellar activity cycle. By analogy with the solar case, such diagrams are interpretable in terms of migration of activity centers towards latitudes with different angular velocities.

The observations presented in Paper I are sufficiently time extended to use stellar butterfly diagrams to investigate the SDR. Since spots cover a limited range of latitudes the SDR amplitudes derived with this method are lower limits. Nonetheless, this method can allow us to investigate the existence of correlations with other global stellar parameters, the existence of different patterns of SDR and how they are connected with the phase of the starspot cycle.

In Sect. 2 we present the seasonal rotational periods obtained by means of the periodogram analysis. We also present the results of the pooled variance analysis we carried out to disentangle the possible effects of the active regions growth and decay (ARGD) on rotational period variations. The existence of different SDR patterns and their correlation

with stellar parameters are discussed in Sect. 3, while the conclusions are presented in Sect. 4.

We refer the reader to Paper I for information on the global properties of the six stars under investigation, on the photometric observations on which the present analysis is based, as well as on data acquisition and reduction procedures.

2. Analysis

2.1. Periodograms

The photometric data of the six program stars were analysed using the Scargle-Press period search routine (Scargle 1982; Horne & Baliunas 1986) to look for the period of the photometric rotational modulation.

The results are summarized in the Tables 2–7, where we list: time interval (HJD range) to which the photometric period refers, number of observations ($N_{\rm m}$), photometric period (P) and its uncertainty (ΔP), as derived from the method of Horne & Baliunas (1986), and the *false-alarm-probability* (FAP) of the peak frequency. The last quantity estimates the probability that a peak of that height could result from a similar sample of Gaussian noise with the same variance of analysed data (cf. Horne & Baliunas 1986). No apparent periodicity was detected in a few seasons, when the data were too few and sparse. The lack of apparent periodicity in other seasons was caused by the rather uniform longitudinal distribution of the spot centers that could not produce a coherent rotational modulation. Secondary periodicities were also searched by filtering the primary frequency modulation from the data and recomputing the periodogram for residual data, according to the prescriptions of Horne & Baliunas (1986) and Baliunas et al. (1995). Only EK Dra showed evidence in several seasons for a significant secondary periodicity in the optical modulation, when the primary frequency was assumed to be real. Once determined the seasonal photometric period, it proved possible to select several time intervals (see Tables 3– 8 of Paper I) along which the flux showed a regular modulation which could be attributed to the rotation of a stationary spot pattern on the photosphere of the star. In such a way 24 light curves were obtained for BE Cet, 18 for k^1 Cet, 35 for π^1 UMa, 92 for EK Dra, 12 for HN Peg and 53 for DX Leo.

The light curves of all program stars showed remarkable variations in shape and amplitude over different time scales. The shortest-term variability can be attributed to optical flaring, whereas the variability observed on time scales of a few rotations may be attributed to sizeable intrinsic changes of the photospheric spot pattern. The longest-term variability, which can be cyclical, is attributable to variations of the total spotted area as well as of its distribution on the stellar photosphere. It has been already analysed in Paper I by running the Scargle-Press routine on the whole sequence of light curves.

Although not included in *The Sun in time* project, we could retrieve from the literature an extended time series of photometric observations also for the single main-sequence star LQ Hya. As done for the six program stars, we analysed the LQ Hya photometric data with the periodogram and determined new seasonal values of the rotational period (Table 8). We also performed a new search for starspot cycles. In fact, we considered the most recent photometry presented by Berdyugina et al. (2002 and references therein) and that collected by the APT80 telescope of Catania Astrophysical Observatory (Rodonò et al. 2001; Messina et al. 2002), which were not yet taken into account in previous starspot cycle studies. Three starspot cycles were found: $P_{\rm cyc1} = 3.2 \pm 0.1$ yr, $P_{\rm cyc2} = 6.2 \pm 0.3$ yr, $P_{\rm cyc3} = 11.4 \pm 0.4$ yr. These cycle periods are consistent with those attained by Oláh & Strassmeier (2002) and supersede the values used in Paper I.

Table 2. BE Cet: time range (HJD-2 440 000) to which the period refers, number of data points (N_m), photometric period and its uncertainty ($P \pm \Delta P$), False-Alarm-Probability (FAP).

HJD range	N_m	$P \pm \Delta P$ (d)	FAP
6736–6761	15	7.744 ± 0.295	0.190
7129–7143	10	7.744 ± 0.134	6.97e-2
7549–7557	9	7.405 ± 0.654	0.176
7869-7876	8	7.477 ± 0.223	0.100
8200–8245	17	8.030 ± 0.198	0.205
8897–8958	33	8.030 ± 0.069	1.02e-3
9234–9353	72	7.804 ± 0.009	5.77e-13
9612–9689	46	7.780 ± 0.027	2.38e-7
11085–11197	62	7.872 ± 0.020	8.08e-9
11 447–11 560	18	7.702 ± 0.051	6.41e-2

Table 3. k^1 Cet.

HJD range	N_m	$P \pm \Delta P$ (d)	FAP
9239–9393	87	9.123 ± 0.019	3.85e-12
9653–9773	41	9.135 ± 0.036	4.20e-5
9986–10040	34	9.367 ± 0.142	3.89e-3
10391–10482	32	9.211 ± 0.024	2.98e-5
10718–10836	27	9.045 ± 0.058	5.43e-2
11 102–11 240	33	9.406 ± 0.039	5.08e-4

Table 4. π^1 UMa.

HJD range	N_m	$P \pm \Delta P$ (d)	FAP
7625–7650	15	5.104 ± 0.176	0.49
8174–8211	14	4.828 ± 0.041	4.50e-2
8230–8361	43	4.670 ± 0.006	3.52e-7
8622–8742	33	4.759 ± 0.008	8.84e-5
9018–9062	15	4.543 ± 0.043	0.223
9284–9398	81	4.661 ± 0.009	2.54e-9
9411–9482	35	4.791 ± 0.023	6.7e-6
9644–9808	94	4.697 ± 0.011	1.47e-4
10 029–10 214	94	4.687 ± 0.009	1.08e-5
10 405–10 517	68	4.795 ± 0.012	4.15e-8
10 736–10 949	102	4.683 ± 0.008	2.17e-5
10 736–10 949	102	5.385 ± 0.009	2.52e-6
11 118–11 296	73	5.294 ± 0.011	2.51e-5
11 546–11 582	17	5.305 ± 0.063	4.19e-2
11 612–11 634	10	5.244 ± 0.107	0.13

Table 5. EK Dra.

HJD range	N_m	$P \pm \Delta P$ (d)	*FAP*	note
5780–5873	9	2.8591 ± 0.0097	0.22	
6187–6250	21	2.8085 ± 0.0880	1.73e-2	
6486–6519	23	2.8864 ± 0.0206	1.55e-2	
6547–6621	24	2.7007 ± 0.0088	1.49e-2	
6881–6982	24	2.8340 ± 0.0085	0.109	
7198–7231	8	2.7418 ± 0.0265	0.325	
7623–7687	48	2.6576 ± 0.0072	5.27e-5	1
7623–7687	48	2.7850 ± 0.0171	0.198	2
7915–8007	30	2.5955 ± 0.0034	2.46e-4	
8045–8065	15	2.8196 ± 0.0193	8.05e-2	
8307–8435	86	2.7843 ± 0.0019	9.68e-13	1
8307–8435	86	2.6365 ± 0.0029	8.34e-8	2
8687–8805	50	2.6016 ± 0.0036	7.99e-5	1
8687–8805	50	2.7959 ± 0.0043	1.48e-4	2
9077–9101	18	2.6220 ± 0.0069	5.14e-3	1
9077–9101	18	2.8831 ± 0.0466	0.28	2
9115–9166	78	2.7936 ± 0.0074	1.70e-9	1
9115–9166	78	2.5714 ± 0.0050	9.80e-11	2
9379–9481	107	2.7773 ± 0.0037	8.41e-11	1
9379–9481	107	2.6056 ± 0.0045	5.15e-7	2
9499–9544	51	2.7796 ± 0.0052	4.11e-8	
9703–9785	27	2.6097 ± 0.0040	5.54e-4	1
9703–9785	27	2.7796 ± 0.0092	3.45e-2	2
9810–9904	36	2.6262 ± 0.0037	4.93e-5	1
9810–9904	36	2.8292 ± 0.0115	0.155	2
10 075–10 100	66	2.7635 ± 0.0084	8.61e-11	1
10 075–10 100	66	2.4906 ± 0.0090	2.56e-9	2
10 143–10 208	36	2.5814 ± 0.0083	1.82e-3	1
10 143–10 208	36	2.8244 ± 0.0089	9.67e-4	2
10 212–10 261	28	2.5955 ± 0.0083	8.06e-4	
10 432–10 583	118	2.5953 ± 0.0015	1.00e-15	1
10 432–10 583	118	2.6576 ± 0.0049	3.98e-3	2
10 590–10 620	20	2.5517 ± 0.020	3.94e-2	1
10 590–10 620	20	2.7960 ± 0.0345	0.177	2
10 822–10 914	30	2.6076 ± 0.0024	6.45e-5	1
10 822–10 914	30	2.5648 ± 0.0090	0.140	2
10 979–10 994	8	2.6310 ± 0.0251	0.119	
11 212–11 266	22	2.7513 ± 0.0120	3.08e-2	1
11 212–11 266	22	2.5504 ± 0.0160	0.187	2
11 623–11 675	29	2.7080 ± 0.0104	1.63e-3	1
11 623–11 675	29	2.5543 ± 0.0145	4.77e-2	2

(1) primary period; (2) after filtering.

Table 6. HN Peg.

HJD range	N_m	$P \pm \Delta P$ (d)	*FAP*
9126–9163	22	4.62 ± 0.05	2.54e-2
9239–9337	22	4.72 ± 0.03	0.19
9491–9547	18	4.73 ± 0.04	5.91e-2
9633–9706	36	4.59 ± 0.02	3.15e-3
9986–10071	29	5.09 ± 0.02	5.73e-4
10 392–10 443	20	5.17 ± 0.05	7.97e-2
10 714–10 806	33	5.15 ± 0.02	5.37e-4
11 010–11 179	64	4.69 ± 0.01	1.47e-2

Table 7. DX Leo.

HJD range	N_m	$P \pm \Delta P$ (d)	*FAP*
7570–7673	63	5.423 ± 0.0059	3.55e-11
8346–8393	18	5.450 ± 0.0240	4.33e-7
8540–8761	27	5.405 ± 0.0100	6.644e-3
8906–9137	102	5.438 ± 0.0059	8.53e-11
9311–9374	50	5.432 ± 0.0410	1.70e-3
9382–9424	31	5.438 ± 0.0200	1.10e-2
9433–9511	110	5.345 ± 0.0157	1.24e-12
9644–9840	126	5.397 ± 0.0051	1.00e-15
9996–10120	96	5.408 ± 0.0044	1.00e-15
10 082–10 216	94	5.420 ± 0.0083	1.49e-12
10 392–10 575	240	5.438 ± 0.0034	1.00e-15
10 728–10 976	143	5.391 ± 0.0039	1.00e-15
11 094–11 159	29	5.444 ± 0.0200	8.54e-4
11 284–11 342	42	5.450 ± 0.0190	5.66e-6
11 546–11 612	17	5.476 ± 0.0100	1.00e-2

Table 8. LQ Hya.

HJD range	N_m	$P \pm \Delta P$ (d)	*FAP*
5683–5725	9	1.5961 ± 0.010	0.4
6023–6178	61	1.5989 ± 0.0010	2.561e-06
7108–7160	30	1.6020 ± 0.0026	2.988e-04
7548–7593	22	1.6133 ± 0.0031	1.836e-03
7881–8030	133	1.5938 ± 0.0013	2.737e-07
8190–8395	64	1.6010 ± 0.0005	8.026e-09
8630–8760	97	1.6081 ± 0.0003	1.00e-15
9324–9496	95	1.6050 ± 0.0005	8.382e-14
9656–9868	116	1.6030 ± 0.0008	1.625e-06
10 004–10 233	234	1.6071 ± 0.0006	2.717e-12
10 387–10 602	754	1.5999 ± 0.0004	1.00e-15
10 731–10 967	181	1.6030 ± 0.0008	1.153e-06
11 101–11 332	154	1.6079 ± 0.0007	4.919e-09
11 501–11 621	119	1.6091 ± 0.0006	1.00e-15
11 831–12 053	235	1.6154 ± 0.0004	1.00e-15
12 195–12 271	48	1.6133 ± 0.0022	2.220e-02

2.2. Pooled variance

The periodogram analysis presented in Sect. 2.1 has allowed us to infer the periodic or quasi-periodic signals attributable to the rotational modulation of visibility of stable spots or spot groups in the stellar photosphere. However, a non-negligible contribution to the detected variability can derive from Active Region Growth and Decay (ARGD). It is interesting to consider the possible effect of active regions' evolution on spurious variations of the photometric period. Dobson et al. (1990), Donahue & Baliunas (1992) and Donahue (1993) have proposed a method, the so-called *pooled variance analysis*, to estimate the time scale of evolution of an active region. This method is based on the analysis of the variance in photometric time series over different time scales. The variance profiles for the program stars have been computed following the Donahue's prescription (1993). The variance profiles are plotted in Fig. 1, while the results are summarized in Table 9 where we list: the star name (Col. 1); the mean semi-amplitudes ($A_{\rm ave}$) of the sinusoidal fits to the observed flux modulation (Col. 2);

the difference between the pooled variance computed at the time scale of rotation ($\sigma^2_{\rm rot}$) and the variance at the shortest measurable time scale ($\sigma^2_{\rm base}$), which gives the semi-amplitude $A_{\rm p} = \sqrt{\sigma^2_{\rm rot} - \sigma^2_{\rm base}}$ (Col. 3); the percent contribution of the rotational modulation of the optical flux over the total variance (Col. 4). The pooled variance profiles of BE Cet, π^1 UMa, EK Dra and DX Leo are similar. The contribution of the rotational modulation to the total variance ranges from 42% to 60%. The pooled variance levels off for time scales longer than the rotation period and it begins increasing again only at about $\log\tau \simeq 2.65$ ($\tau \sim 450$ days), $\log\tau \simeq 2.2$ ($\tau \sim 160$ days) and $\log\tau \simeq 2.7$ ($\tau \sim 500$ days) for BE Cet, π^1 UMa and EK Dra, respectively. In the case of DX Leo, the variance increase occurs at about $\log\tau \simeq 2.4$ ($\tau \sim 250$ days). According to the classification by Donahue et al. (1997a,b) the cited stars are *stars with distinct plateau*, which is the most frequent case among solar-type stars. The existence of a plateau in the pooled variance profile occurring at τ greater than $P_{\rm rot}$ enables us to distinguish the time scales over which the ARGD gives the strongest contribution. In the present case, the time scale at which the evolution of active regions begins to affect the variance of the observed flux ranges from ≃5 months (≃30 rotational periods) to ≃16 months (≃180 rotational periods) for π^1 UMa and EK Dra, respectively. Therefore, we are confident that the rotational periods detected by the periodogram for these stars are entirely attributable to the rotation of stable spot patterns. The maximum value of σ^2 occurs at the $\log\tau$ corresponding to the activity cycle length. In the case of π^1 UMa, a secondary relative maximum is seen at $\log\tau$ corresponding to the secondary activity cycle. The range in $\log\tau$ beyond the rotational plateau indicates the lifetime of active regions complexes, which is of the order of months to years.

The pooled variance profiles of k^1 Cet and HN Peg differ from the previous profiles. In fact, they do not level off for time scales longer than the rotational period. The profile continues to increase monotonically in the case of k^1 Cet, while it levels off at about $\log\tau \simeq 1.5$ in the case of HN Peg. According to Donahue et al.'s classification, such stars belong to *AR evolution-dominated stars*, the less frequent case among solar-type stars. Such a behaviour may indicate that the active region evolution is not sufficiently distincted from the rotational period and it contributes to the pooled variance on a comparable time scale. A much steeper increase of σ^2 occurs near the activity cycle time scale. It is interesting to mention that the pooled variance profile of k^1 Cet, determined by Donahue et al. (1997a,b) and based on Mt. Wilson CaII H&K measurements, has a plateau. k^1 Cet was accordingly classified as a *star with distinct plateau* with a time scale of ≃90 days for the onset of a contribution of ARGD to the total variance.

Figure 2 shows the variance profile of LQ Hya. This star results to be AR *evolution-dominated* with a variance profile similar to the HN Peg's profile. The value of σ^2 increases monotonically for time scales longer than the rotation period. The profile has a plateau starting from $\log\tau \simeq 1.3$ and relative maxima corresponding to the three starspot cycles.

Table 9. Mean semi-amplitude of the sinusoidal fit to the observed flux modulation ($A_{\rm ave}$), semi-amplitude ($A_{\rm p}$) and relative contribution ($\sigma_{\rm rot}/\sigma_{\rm tot}$) of rotation to the observed total variance.

Star	$A_{\rm ave}$	$A_{\rm p} = \sqrt{\sigma^2_{\rm rot} - \sigma^2_{\rm base}}$	$\sigma_{\rm rot}/\sigma_{\rm tot}$
BE Cet	0.0147	0.0089	60%
k^1 Cet	0.0134	0.0055	49%
π^1 UMa	0.0119	0.0050	42%
EK Dra	0.0327	0.0130	40%
HN Peg	0.0110	0.0060	20%
DX Leo	0.0284	0.0141	50%
LQ Hya	0.0540	0.0050	13%

3. Discussion

3.1. Surface differential rotation patterns

The quasi-periodic brightness variations on time scales of the order of the rotational period can be thus attributed to the photospheric starspot centers whose visibility is modulated by the stellar rotation. The modulation period marks the angular velocity of the latitudes at which the starspot activity is predominantly centered. By analogy with the solar case, the year-to-year variations of the rotational period can be attributed to the migration of stellar activity centers towards latitudes possessing different angular velocity. Such migration is caused by the internal radial shear to which the observed latitudinal shear is coupled as assumed e.g. in the $\alpha - \Omega$ dynamo.

To date the most extensive observational study of SDR is based on rotational period variations derived from CaII H&K flux measurements at Mt. Wilson (Donahue 1993; Donahue et al. 1996 and references therein). Evidence of SDR is found in 37 stars (including the Sun), over a sample of nearly 100 lower main-sequence stars (Donahue et al. 1996). The amplitude of the rotational period variations is found to be dependent on the mean period with a power law and to be independent of the mass. The extended time series of Ca II H&K fluxes measurements have revealed for the first time the existence of stellar butterfly diagrams and allowed us to investigate the correlation between the patterns of such period variations and the level of activity or, when present, the activity cycle phase. Twenty stars out of 37 show different patterns of rotational period variations. These are classified by Donahue & Baliunas (1994) into four different categories: 1) stars with solar-like (or β Com-like) pattern, such as β Com (Donahue & Baliunas 1992) and HD 160346 (Donahue 1996); 2) stars with antisolar pattern, such as HD 10476 (Donahue 1996); 3) stars with switching patterns (from solar to antisolar or the reverse at about middle cycle phase) (Donahue et al. 1996); 4) stars with two well-separated active latitudes, such as χ^1 Ori (Donahue & Baliunas 1994). The remaining 15 stars do not show any recognizable pattern, although four of them have well-defined cycles.

Another observational study of SDR based on long-term photometry has been presented first by Hall (1991). He analysed a sample of 86 variable stars of different types (including the Sun) and determined rotational period variations from

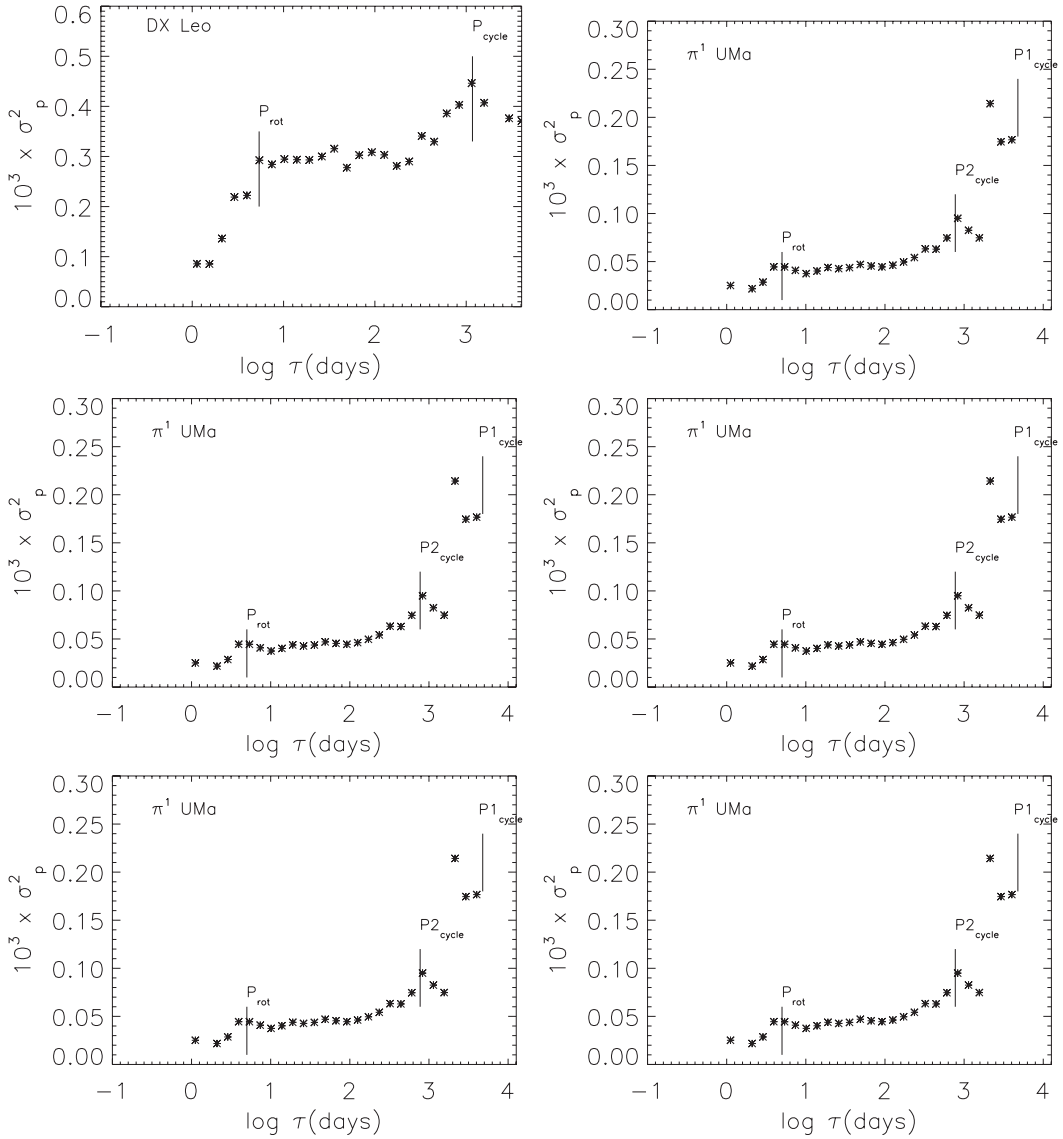

Fig. 1. Pooled variance profiles for program stars. The time scales of the rotation period modulation and of activity cycles are indicated by vertical bars. DX Leo, π^1 UMa, EK Dra and BE Cet are *stars with distinct plateau* according to Donahue et al. (1997a,b), while HN Peg and k^1 Cet are *AR evolution-dominated stars*.

O−C plots, where "O" is the observed time of light minimum and "C" is the time computed with an arbitrarily assumed rotational period. He found that the amplitude of SDR is correlated with the rotational period by a power law (rapidly rotating stars approaching solid-body rotation) and with the lobe-filling factor (less differential rotation for stars which nearly fill their Roche lobes). Henry et al. (1995) extended the analysis to a larger sample of 90 stars, including as single main-sequence stars only the Sun, ϵ Eri and likely HD 191011. The existence of a correlation between rotational period variations and long-term brightness changes was detected in five stars (four binaries and one subgiant star).

The extended time series of photometric data collected as part of *The Sun in time* project allows us to investigate in a selected sample of single solar-type stars the existence of those SDR patterns already detected by Donahue from Ca II H&K fluxes measurements and by Henry et al. from O−C plots in

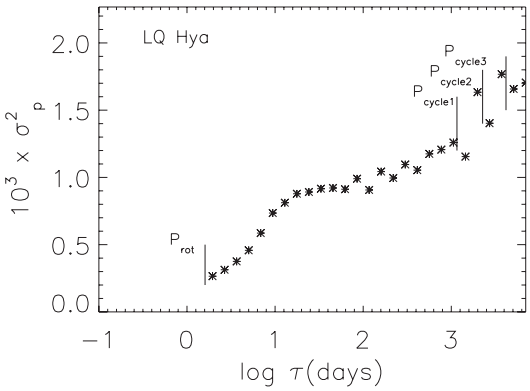

Fig. 2. As in Fig. 1, but for LQ Hya.

binary and subgiant stars. In such a way analogies and/or differences with respect to the solar case and to binary stars can

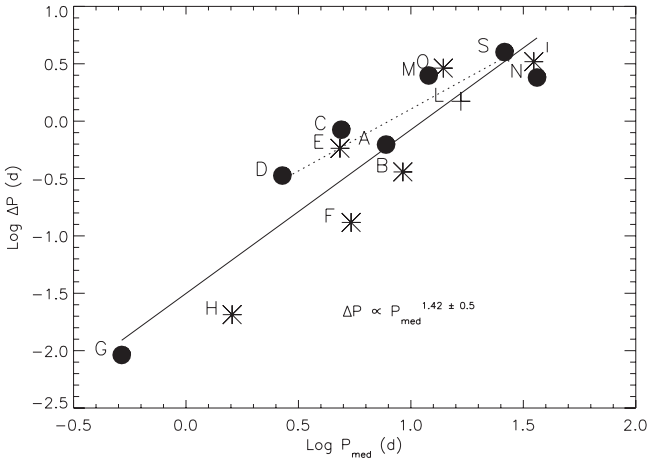

Fig. 3. The rotational period variations (ΔP) for the stars in Table 1 are plotted vs. the mean rotational period. Bullets, asterisks and pluses denote solar, antisolar and hybrid SDR patterns, respectively. Capital letters identify the targets according to Table 1. The continuous line is a power law fit to the whole sample, while the dotted line is a power law fit to G-type stars only.

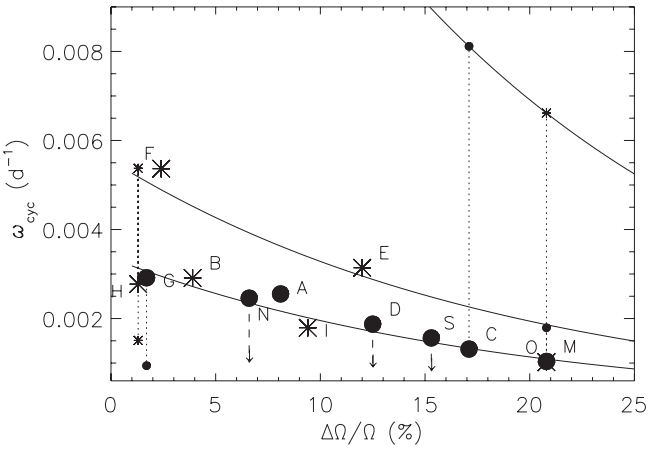

Fig. 5. The cycle frequency (ω_{cyc}) is plotted vs. the relative surface differential rotation amplitude ($\Delta\Omega/\Omega$). Stars tend to concentrate along three different branches. Vertical dotted lines connect multiple cycles. The dashed arrows for targets D, S and N indicate the existence of a long-term trend superimposed on the detected cycle. Symbols and labels have the same meaning as in Fig. 3.

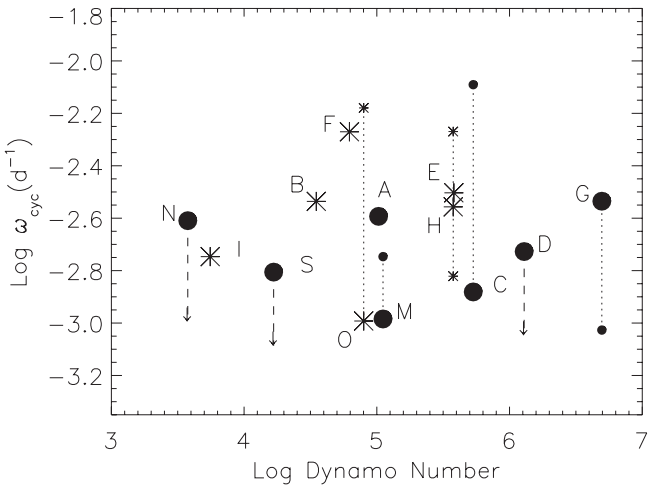

Fig. 4. The cycle frequency ($\omega_{\rm cyc}$) is plotted vs. the Dynamo Number (D). Dotted lines and capital letters have the same meaning as in Fig. 3.

be investigated. Preliminary results based on photometric data were presented by Messina et al. (1999) and Messina & Guinan (2001).

In Figs. 6–12 (top panels) we plot the time sequence of V-band magnitudes of the program stars. Dots are nightly averaged observations and diamonds are mean magnitudes computed from individual light curves ($V_{\rm max} + V_{\rm min}$)/2. Continuous lines are sinusoidal fits to the data according to the cycle periods listed in Table 1 (see also Sects. 3 and 4 of Paper I). In the bottom panels of Figs. 6–12 we plot the seasonal values of the rotational period and their uncertainty as listed in Tables 2–8. Continuous lines are linear fits to the data. Horizontal lines show the time location of individual starspot cycles and show the correlation between the trend of rotational period variations and the starspot cycle phase.

In the case of BE Cet and π^1 UMa (Figs. 6 and 7) the rotational period tends to decrease steadily during each cycle, jumping back to a higher value at the beginning of a new cycle. This is reminiscent of the sunspot cyclic behaviour, where the latitude of spot formation moves toward the equator, i.e., toward progressively faster rotating latitudes along an activity cycle, thus producing a decrease in the photometric period. However, the rotational period measurements of π^1 UMa are at present limited to less than two cycles and future observations are needed to confirm the solar-like behaviour. In the case of EK Dra (Fig. 8) the periodogram analysis detected the presence of a secondary rotation period in several seasons, as mentioned in Sect. 2.1. Both periods tend to decrease steadily during 17 yr of observations. The two contemporary rotational periods are likely to be due to the presence of two long-lived active regions at different latitudes with different angular velocities because of the differential rotation regime. The period variations seem to be correlated with the long-term photometric variation. On the basis of a recent study of long-term photometry on Sonneberg sky-patrol plates (Fröhlich et al. 2002), this long-term variation may be a segment of a cycle longer than half a century. If this is the case, EK Dra would display a solar-like behaviour.

k^1 Cet, HN Peg and DX Leo (Figs. 9 to 11) show an antisolar pattern, where the rotational period tends to increase steadily during each cycle, jumping back to a lower value at the beginning of a new cycle. In the case of k^1 Cet, we have to date measurements of the rotational period along one starspot cycle only, while in the case of HN Peg the last rotational period measured at the epoch 1998.23 seems to confirm the suspected antisolar behaviour. It is important to remember that the pooled variance analysis has shown that for k^1 Cet and HN Peg the ARGD may affect the value of the rotational period. Therefore, on the basis of the available relatively sparse rotational period data and of the pooled variance analysis, we reserve to confirm the antisolar behaviour of these two stars with future observations. On the contrary, in the case of DX Leo (Fig. 11) the number of observed starspot cycles is sufficient to confidently classify its behaviour as antisolar.

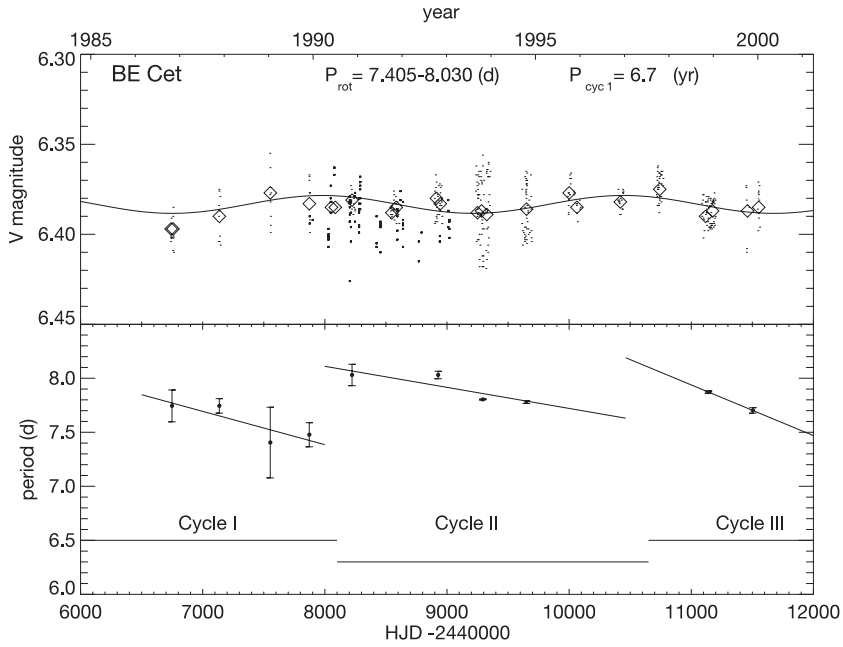

Fig. 6. (*Top panel*) Long-term *V*-band brightness variations of BE Cet. The modulation is fitted by a sinusoid with period of $P_{\rm cyc}$ = 6.7 yr. (*Bottom panel*) Seasonal rotation periods vs. time with a linear fit to data. The rotation period monotonically decreases along the starspot cycle showing a solar-like behaviour.

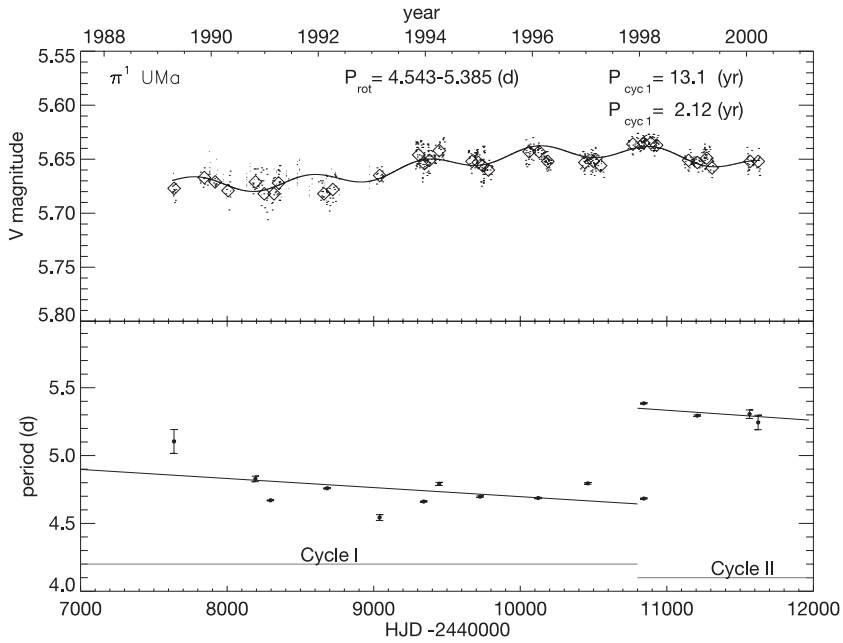

Fig. 7. (*Top panel*) Long-term *V*-band brightness variations of π^1 UMa. The modulation is fitted by a sinusoid with two periods: of $P_{\rm cyc1}$ = 13.1 yr and $P_{\rm cyc2}$ = 2.12 yr. (*Bottom panel*) Seasonal rotation periods vs. time with a linear fit to data. The rotation period monotonically decreases along the starspot cycle showing a solar-like behaviour.

LQ Hya (Fig. 12) has a rotational period which varies in phase with the 6.2-yr starspot cycle and with a clear antisolar behaviour. It is remarkable that a regular and photometrically detectable pattern of SDR persists, although three cycles with similar amplitude (0.02 mag) and different period superimpose each on other.

It is also interesting to note that the slope of the rotational period variations and, therefore, the amplitude of SDR changes from cycle to cycle. Such behaviour is evident for BE Cet and best visible for DX Leo and LQ Hya whose photometric monitoring cover several cycles. Such behaviour, already observed in AB Dor (Collier Cameron & Donati 2002) from spectroscopic data, resembles a wave of excess rotation on a time scale of the order of decades. However, the observed variation of the slope from cycle to cycle may as well as be caused by a variation of the width of the latitude band in which spots occur.

One of the most remarkable results derived from this analysis is the indirect evidence (since the stellar disk is not spatially

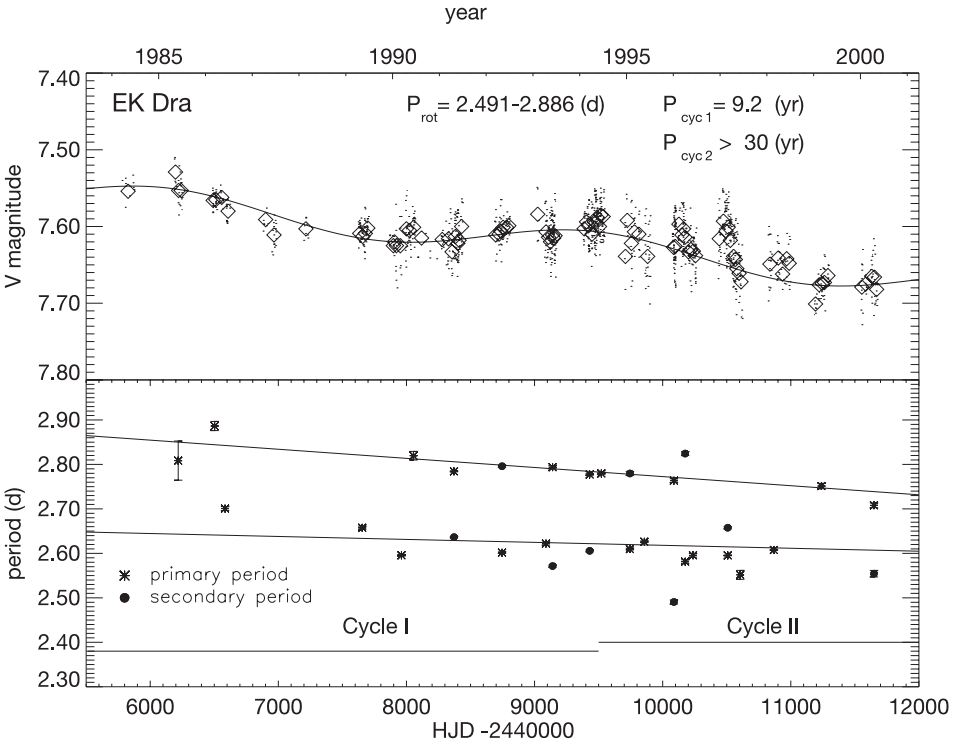

Fig. 8. (*Top panel*) Long-term V-band brightness variations of EK Dra. The modulation is fitted by a sinusoid with a period of $P_{\rm cyc}$ = 9.2 yr plus a longer term trend ($P_{\rm cyc} \geq 30$ yr if cyclic). (*Bottom panel*) Seasonal rotation periods vs. time with linear fits to data. Two rotation periods were detected in several seasons, both showing monotonical decreases along each starspot cycle with solar-like behaviour.

resolved), also from photometric data, that solar-type stars can display an antisolar pattern of SDR in the sense of rotational periods steadily increasing during the starspot cycle. In the case of the Sun, the migration of active regions is regarded as a consequence of the latitudinal migration of a dynamo wave propagating in a shell near the base of the solar convective zone. The direction of migration is related to the sign of the product of the radial gradient of the angular velocity in the shell $\frac{\partial\Omega}{\partial r}$ by the parameter α, which measures the intensity of the regeneration of the poloidal field component by cyclonic convection (Moffatt 1978)[1]. In the Sun the sign of $\alpha\frac{\partial\Omega}{\partial r}$, at low and intermediate latitudes, is such as to produce an equatorialward migration of the dynamo wave (Stix 1976). Such a migration, in association with the increase in the angular velocity toward the equator ($\frac{\partial\Omega}{\partial\phi} < 0$, where ϕ is the latitude), is responsible of the decrease in the rotational period of the active regions of the Sun versus increasing cycle phases, i.e toward the activity maximum.

In order to explain the antisolar behaviour observed in stars with Sun-like global properties, a different pattern of the differential rotation (or of the α effect) might be invoked, i.e. a poleward acceleration of the surface differential rotation. However, it is also possible to propose an interpretation in terms of high latitude starspot activity with the same internal differential rotation pattern of the Sun. Specifically, helioseismic observations show that the radial gradient at the base of the convective zone $\frac{\partial\Omega}{\partial r}$ changes sign for $\phi > 40°$ (e.g., Kosovichev 1996). The solar dynamo is not strong enough to produce spot activity at latitudes $\phi > 40°$, but in more active stars the dynamo may be expected to amplify significantly the toroidal field up to subpolar latitudes (e.g., Tobias et al. 1997; Belvedere et al. 1998). The high latitude spot belts ($\phi > 40°$) will migrate toward the pole, because the sign of $\alpha\frac{\partial\Omega}{\partial r}$ is opposite to that in low latitudes ($\phi < 40°$), and if the rotation axis of the star is inclined with respect to the line of sight, the high latitude spots may well dominate the optical modulation producing an increase in the photometric period with the activity cycle phase.

Evidence of periodic variations of the rotational period correlated with the starspot cycle phase are also found in binary stars, e.g. in the RS CVn-type star II Peg (Rodonò et al. 2000), which displays a solar-like SDR pattern. An undergoing study, based on long-term photometry of binary stars (Rodonò et al. 2003) and carried out in a consistent way as that used in the present analysis, will allow us to investigate analogies and/or differences with respect to the case of single main-sequence stars.

3.2. Correlation with stellar parameters

In order to perform a more robust analysis of the correlation between SDR and global stellar properties, we searched the literature for other stars with known cycles and contemporary seasonal rotational period determinations. Eight stars were found to satisfy our requirements: AB Dor, 107 Psc, 61 UMa, β Com, HD160346, 15 Sge and the Sun. These stars are listed in Table 1

[1] In the present discussion we shall assume that any possible meridional flow does not affect significantly the migration of the dynamo wave in the Sun and active stars.

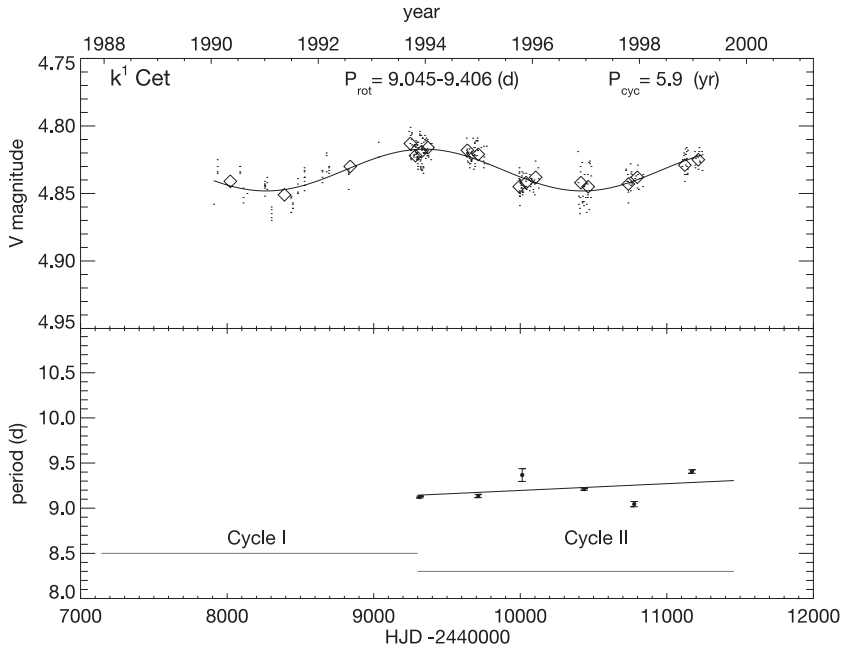

Fig. 9. (*Top panel*) Long-term *V*-band brightness variations of k^1 Cet. The modulation is fitted by a sinusoid with a period of P_{cyc} = 5.9 yr. (*Bottom panel*) Seasonal rotation periods vs. time with a linear fit to data. The rotation period monotonically increases along the starspot cycle showing an anti solar-like behaviour.

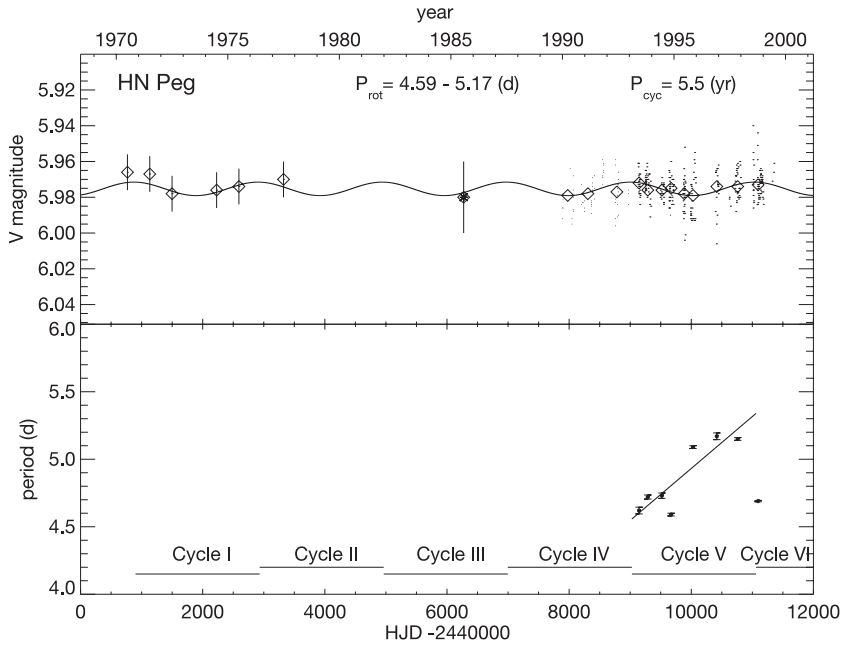

Fig. 10. (*Top panel*) Long-term *V*-band brightness variations of HN Peg. The modulation is fitted by a sinusoid with a period of P_{cyc} = 5.5 yr. (*Bottom panel*) Seasonal rotation periods vs. time with a linear fits to data. The rotation period monotonically decreases along the starspot cycle showing a solar-like behaviour.

with indication of the type of database (photometry or CaII H&K fluxes) from which the activity cycle and the rotational period are determined. Actually, 61 UMa has not a detectable cycle but only a long-term trend and is the only star in our sample which displays a hybrid pattern of SDR, that is it is not possible to clearly identify a solar or an antisolar behaviour.

Dynamo models make assumptions on the dependence of SDR on the stellar rotational period. Such assumptions differ on the basis of the hypotheses and physical effects they try to parameterize. Our attention is presently focused on Kitchatinov & Rüdiger's (1999) models, according to which a positive correlation exists between the absolute value of SDR and the stellar rotation period according to a power law

$$\Delta P \propto P^n. \quad (1)$$

Kitchatinov & Rüdiger (1999) found that the power index n is neither constant with rotation rate nor with spectral type. More precisely, n decreases vs. faster rotation regimes (from n = 2.56

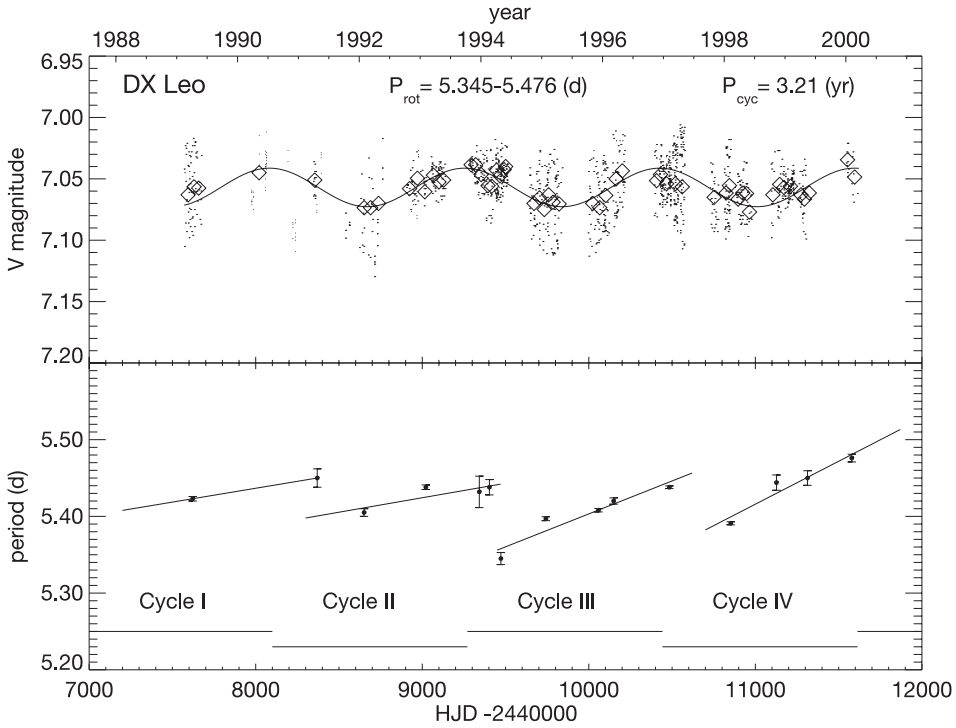

Fig. 11. (*Top panel*) Long-term V-band brightness variations of DX Leo. The modulation is fitted by a sinusoid with a period of $P_{\rm cyc}$ = 3.21 yr. (*Bottom panel*) Seasonal rotation periods vs. time with a linear fits to data. The rotation period monotonically increases along each starspot cycle showing an anti solar-like behaviour.

for the solar rotation to $n = 2$ for $P_{\rm rot} = 1$ d) and it is smaller for K5-stars as compared to G2-stars. This power law dependence is confirmed by observational data, although the observational and theoretical values of the power index differ.

Figure 3 shows the amplitude $\Delta P (= P_{\rm max} - P_{\rm min})$ of the rotational period variations vs. the mean rotation period for our sample totalling 14 targets with known activity cycles and SDR. Different symbols denote the solar (bullets), antisolar (asterisks) or hybrid (pluses) SDR patterns, while capital letters identify the targets according to Col. 12 of Table 1. We found a power law dependence with index $n = 1.42 \pm 0.5$ (continuous line in Fig. 3) in fair agreement with the observational value $n = 1.30$ reported by Donahue et al. (1996) and $n = 1.15-1.30$ by Rüdiger et al. (1998). The agreement is even better when we consider that the ΔP values are lower limits and those we determined for pole-on stars are underestimated more than for equator-on stars. In fact, in almost pole-on stars low-latitude spots are not visible and high-latitude spots determine almost flat light curves; therefore, the photometric rotational period can be determined from spots within a latitude range more limited than in almost equator-on stars, whose spots are visible at all latitudes. Therefore, if we assume that antisolar stars (asterisks in Fig. 3) are almost pole-on stars, their values are more underestimated than the values represented by the bullets. We found $n = 1.30$ by increasing ΔP for antisolar stars by ∼10%

The disagreement between the observational (n = 1.15–1.30) and the theoretical ($n > 2$) values are attributed by Kitchatinov & Rüdiger (1999) to the different spectral types present in Donahue et al.'s sample (1996). However, if we select the G-type stars only from our sample, the corresponding power index (dotted line in Fig. 3) slightly changes to the value $n = 1.08$, making the disagreement even larger. Consistently with the theoretical predictions, we find that the SDR amplitude for K-type stars is smaller if compared to G-type stars.

The $\alpha-\Omega$ dynamo theory makes predictions also on the dependence of the cycle frequency ($\omega_{\rm cyc}$) on the Dynamo Number (D), which is the most important parameter controlling the magnetic field generation and evolution in mean field dynamo models. The cycle frequency ($\omega_{\rm cyc}$) is expected to scale with D as

$$\omega_{\rm cyc} \propto D^m. \qquad (2)$$

The value of the m index depends on the type of dynamo which is supposed to operate. For example, m is between 1/3 (Noyes et al. 1984) and 1/2 (Moss et al. 1990) in standard distributed dynamos. The dependence on D becomes very weak, the value of m decreasing down to 1/6 (see Brandenburg et al. 1994) in the case of an overshoot layer dynamo. The m index varies also according to the nonlinearities introduced in the model (e.g., α-quenching or flux-loss).

The newly determined values of cycle frequency from Paper I and the relative amplitudes of SDR here presented, along with those already known from previous studies (see Table 1), enable us to check the validity of Eq. (2) on observational ground, more precisely, by a semi-empirical determination of the Dynamo Number.

We adopt the definition of Brandenburg et al. (1994) for the Dynamo Number

$$D = \alpha \Omega' R_\star^4 / \eta_T^2 \qquad (3)$$

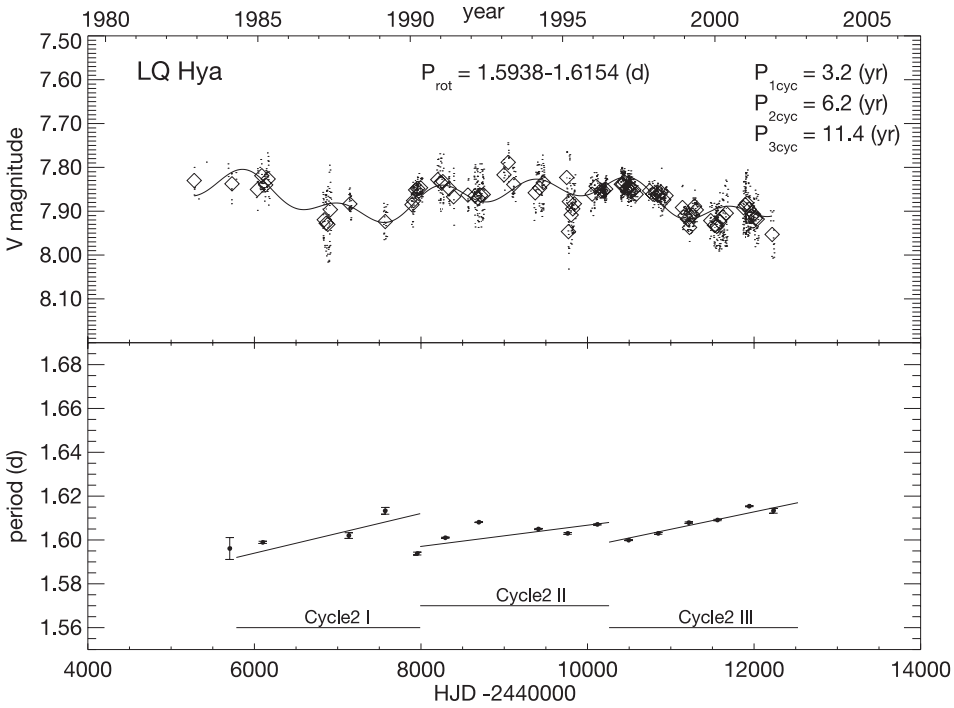

Fig. 12. (*Top panel*) Long-term *V*-band brightness variations of LQ Hya. The modulation is fitted by a sinusoid with three periods $P_{\rm cyc1}$ = 3.2 yr, $P_{\rm cyc2}$ = 6.2 yr, $P_{\rm cyc3}$ = 11.4 yr. (*Bottom panel*) Seasonal rotation periods vs. time. The rotation period varies with the 6.2-yr cycle. An antisolar behaviour is apparent.

where α is the helicity ($\propto \Omega l$, where l is the mixing length at the base of the convective zone), Ω' is the differential rotation ($=|\nabla\Omega| = \Delta\Omega/R_\star$), $R_\star$ the stellar radius and η_T the coefficient of the turbulent diffusion ($=\frac{1}{3}\overline{v}_{\rm c} l$, where $\overline{v}_{\rm c}$ is the mean convective velocity). Since $\overline{v}_{\rm c} = l/\tau_{\rm c}$, D can be rewritten as

$$D = 9\tau_{\rm c}^2 \Omega \Delta\Omega (R_\star/l)^3. \quad (4)$$

The values of $\tau_{\rm c}$, $l = \alpha H_p$ and $R_\star$ are computed from Girardi et al.'s (2000) models.

As shown in Fig. 4, $\omega_{\rm cyc}$ and D appear to be very poorly correlated nor the dependence predicted in Eq. (2) can be certainly inferred from these observational data. When we consider the high level of parameterization, it should not be surprising that models are able to reproduce empirical relations as Eq. (1), while they fail to predict relations between other observational quantities under the same assumptions.

Actually, the quantity we found to be highly correlated to the cycle frequency is the relative surface differential rotation amplitude ($\Delta\Omega/\Omega$).

Figure 5 shows cycle frequency ($\omega_{\rm cyc}$) vs. $\Delta\Omega/\Omega$. We can see that the cycle frequency increases with increasing SDR amplitude and stars seem to concentrate along three different branches. The best fit to data is given by exponential laws

$$\omega_{\rm cyc} = a \cdot {\rm e}^{b\,\frac{\Delta\Omega}{\Omega}} \quad (5)$$

(continuous lines of Fig. 5). All the three branches have the same coefficient $b = -0.055 \pm 0.004$. It is important to note that any tentative power law fit failed. Vertical dotted lines connect multiple cycles, while dashed arrows for targets D, S and N are used to indicate the existence of a longer-term trend superimposed on the primary cycle (see Table 1). No significative difference was found in the results when we tried to increase the $\Delta\Omega$ values of antisolar stars by ∼10% as already discussed.

On the basis of these observational results, the Dynamo number does not appear to be the best parameter to describe the magnetic field generation, at least in the $\alpha - \Omega$ dynamo formulation. The magnetic amplification mechanism, that is the differential rotation in the form $\Delta\Omega/\Omega$, seems to be the key parameter controlling the duration of the magnetic cycle.

Since stars with solar (bullets) or antisolar (asterisks) patterns generally behave in the same manner as shown in Figs. 3–5, the same type of dynamo may operate in these apparently different classes of stars. Therefore, a different angle of sight from which these stars are observed from Earth seems to be the only and most reasonable explanation (see. Sect. 3.2) for the different shape in the correlation between the cycle phase and cyclic rotational period variations. More precisely, solar patterns are observed in almost equator-on stars, antisolar pattern in almost pole-on stars. Unfortunately, we have no photometric data to interpret the hybrid behaviour shown by the star 61 UMa.

4. Conclusions

Extended time series of high precision photometric measurements can provide relevant information on the presence and characteristics of the surface differential rotation in late-type stars. The analysis we performed on a sample consisting of six young solar analogues, observed as part of *The Sun in Time*,

and of eight additional single main-sequence stars, with known activity cycles and SDR amplitude, allowed us to infer the following results:

– All the targets show changes in the seasonal rotational periods. Such changes are strictly periodic and in phase with the starspot cycle for BE Cet, DX Leo and LQ Hya. Such changes are also probably both periodic and in phase with the starspot cycle in the case of π^1 UMa, EK Dra and HN Peg. However, the rotational period measurements for these stars are at present sparse and limited to less than two starspot cycles. Future observations are needed to confirm the expected behaviour. In the case of k^1 Cet, the rotational period variations are in phase with the starspot cycle, but limited to only one cycle. It is not yet possible to assess the SDR pattern of this star.

– The pooled variance analysis shows that BE Cet, π^1 UMa, EK Dra and DX Leo are *stars with distinct plateau* and with time scale of evolution of the active regions ranging from $\simeq$5 to $\simeq$16 months. k^1 Cet, HN Peg and LQ Hya are *AR evolution-dominated stars* with time scale of evolution of the active regions comparable to the rotation period.

– The rotational period changes are consistent with the presence of SDR and attributable to the migration of the activity centers during the activity cycle toward latitudes shearing different angular velocities. Figures 6–12 show the existence of two different patterns of correlation between the starspot cycle phase and the rotational period variations: *i*) a solar-like pattern for BE Cet, π^1 UMa, EK Dra, which is reminiscent of the solar behaviour; *ii*) an antisolar-like pattern for DX Leo, LQ Hya, HN Peg and for k^1 Cet to be confirmed.

– The rotational period variations (ΔP) scale with rotational period according to a power law with exponent $n = 1.42$, which is in fair agreement with the results of previous studies. The agreement is even better ($n = 1.30$) when we consider that the ΔP values of antisolar stars may be underestimated by a $\sim$10% more than the values of solar stars. The new estimates of cycle period presented in Paper I and the new values of SDR amplitude allowed us to find that the cycle frequency is correlated to high degree to the relative amplitude of the SDR. Stars tend to concentrate along three branches according to an exponential law with coefficient $b = -0.05$. The lack of correlation with a semiempirically determined Dynamo Number seems to indicate that the differential rotation, and therefore the magnetic field amplification mechanism, is the key quantity controlling the activity cycle period rather than the turbulent diffusion.

– No difference is observed among stars with solar and antisolar SDR patterns for what concerns the correlations between the amplitude of the period variation and the rotation period or between the cycle frequency and the relative surface differential rotation amplitude. The apparently different solar and antisolar behaviours are probably due to a different inclination of the stellar rotation axis: almost equator-on stars show a solar SDR pattern; almost pole-on stars show an antisolar SDR pattern.

Acknowledgements. The extensive use of the SIMBAD and ADS databases operated by the CDS center, Strasbourg, France, is gratefully acknowledged. The authors wish to thank an anonymous Referee for a careful reading of the manuscript and valuable comments.
Active star research at the Catania Astrophysical Observatory, INAF, is funded by MIUR (*Ministero dell'Istruzione, dell'Università e della Ricerca*) and the *Regione Siciliana*, whose financial support is gratefully acknowledged. This research is also supported by the US National Science Foundation for Research whose financial support is gratefully acknowledged.

References

Baliunas, S. L., Horne, J. H., Porter, A., et al. 1985, ApJ, 294, 310
Baliunas, S. L., Donahue, R. A., Soon, W. H., et al. 1995, ApJ, 438, 269
Belvedere, G., Lanza, A. F., & Sokoloff, D. 1998, Sol. Phys., 183, 435
Berdyugina, S. V., Pelt, J., & Tuominen, I. 2002, A&A, 394, 505
Brandenburg, A., & Charbonneau, P. 1994 in The Eighth Cambridge Workshop on Cool Stars, Stellar Systems, and the Sun, ed. J.-P. Caillault, ASP Conf. Ser., 64, 354
Catalano, S., Lanzafame, A., Pagano, I., & Rodonò, M. 1999, Mem. Soc. Astron. Ital., 70, 463
Collier Cameron, A., & Donati, J.-F. 2002, MNRAS, 329, L23
Collier Cameron, A., Donati, J.-F., & Semel, M. 2002, MNRAS, 330, 699
Dobson, A. K., Donahue, R. A., Radick, R. R., & Kadlec, K. L. 1990, in The Sixth Cambridge Symposium on Cool Stars, Stellar Systems and the Sun, ed. G. Wallerstein, ASP Conf. Ser., 9, 132
Donahue, R. A. 1993, Ph.D. Thesis, New Mexico State University
Donahue, R. A. 1996, in Stellar Surface Structures, ed. K. Strassmeier, & J. L. Linsky (Dordrecht, Kluwer), IAU Symp., 176, 261
Donahue, R. A., & Baliunas, S. L. 1992, ApJ, 393, L63
Donahue, R. A., & Baliunas, S. L. 1994, in The Eighth Cambridge Workshop on Cool Stars, Stellar Systems, and the Sun, ed. J.-P. Caillault, ASP Conf. Ser., 64, 468
Donahue, R. A., Saar, S. H., & Baliunas, S. L. 1996, ApJ, 466, 384
Donahue, R. A., Dobson, A. K., & Baliunas, S. L. 1997a, Sol. Phys., 171, 211
Donahue, R. A., Dobson, A. K., & Baliunas, S. L. 1997b, Sol. Phys., 171, 191
Donati, J.-F., Mengel, M., Carter, B. D., et al. 2000, MNRAS, 316, 699
Dorren, J. D., & Guinan, E. F. 1994, ApJ, 428, 805
Fekel, F. C., Bopp, B. W., & Africano, J. L. 1986, AJ, 92, 1150
Fröhlich, H.-E., Tschäpe, R., Rüdiger, G., & Strassmeier, K. G. 2002, A&A, 391, 659
Girardi, L., Bressan, A., Bertelli, G., & Chiosi, C. 2000, A&AS, 141, 371
Gray, F. D., & Baliunas, S.L. 1997, ApJ, 475, 303
Güdel, M., Guinan, E. F., & Skinner, S. L. 1997, ApJ, 483, 947
Guinan, E. F., & Giménez, A. 1992, in The Realm of Interacting Binary Stars, ed. J. Sahade, G. E. McCluskey, & Yoji Kondo (Astrophysics and Space Science Library), 177, 51
Guinan, E. F., Ribas, I., & Harper, G. M. 2001, AAS, 199, 8805
Hall, D. S. 1991, in The Sun and Cool Stars. Activity, Magnetism, Dynamos, ed. I. Tuominen, D. Moss, & G. Rüdiger, IAU Coll., 130, 353
Henry, G. W., Fekel, F. C., & Hall, D. S. 1995, AJ, 110, 2926
Horne, J. H., & Baliunas, S. L. 1986, ApJ, 302, 757

Kitchatinov, L. L., & Rüdiger, G. 1999, A&A, 344, 911
Kosovichev, A. G. 1996, ApJ, 469, L61
Messina, S., Guinan, E. F., Lanza, A. F., & Ambruster, C. 1999, A&A, 347, 249
Messina, S., & Guinan, E. F. 2001, in The 12th Cambridge Workshop on Cool Stars Stellar Systems and the Sun, ed. A. Brown, G. M. Harper, & T. R. Ayres Boulder, CO, 06.07
Messina, S., & Guinan, E. F. 2002, A&A, 393, 225 (Paper I)
Moffatt, H. K. 1978, Magnetic Field Generation in Electrically Conducting Fluids (Cambridge: Cambridge Univ. Press)
Moss, D., Tuominen, I., & Brandenburg, A. 1990, A&A, 228, 284
Noyes, R. W., Weiss, N. O., & Vaughan, A. H. 1984, ApJ, 287, 769
Oláh, K., Kolláth, Z., & Strassmeier, K. G. 2000, A&A, 356, 643
Oláh, K., & Strassmeier, K. G. 2002, AN, 323, 361
Reiners, A., & Schmitt, J. H. M. M. 2002, A&A, 384, 155
Rodonò, M. 2000, in Stellar Clusters and Associations: Convection, Rotation, and Dynamos, ed. R. Pallavicini, G. Micela, & S. Sciortino, ASP Conf. Ser., 198, 391
Rodonò, M., Messina, S., Lanza, A. F., Cutispoto, G., & Teriaca, L. 2000, A&A, 358, 624
Rodonò, M., Cutispoto, G., Lanza, A. F., & Messina, S. 2001, AN, 322, 333
Rodonò, M., Messina, S., & Cutispoto, G. 2003, in progress
Rüdiger, G., von Rekowski, B., Donahue, R. A., & Baliunas, S. L. 1998, ApJ, 494, 691
Scargle, J. D. 1982, ApJ, 263, 835
Stix, M. 1976, A&A, 47, 243
Stix, M. 1984, AN, 305, 215
Strassmeier, K. G., Serkowitsch, E., & Granzer, T. 1999, A&AS, 140, 29
Strassmeier, K. G., Bartus, J., Cutispoto, G., & Rodonò, M. 1997, A&AS, 125, 11
Tobias, S. M., Proctor, M. R. E., & Knobloch, E. 1997, A&A, 318, L55
Vogt, S. S., & Penrod, G. P. 1983, PASP, 95, 565
Wilson, O. C. 1978, ApJ, 226, 379